Radioprotection 49(4), 249-256 (2014)

DOI: 10.1051/radiopro/2014014

Available online at:
www.radioprotection.org

Article

The contributions of source regions to organ doses from incorporated radioactive iodine

E. Hoseinian-Azghadi, L. Rafat-Motavalli and H. Miri-Hakimabad*

Physics Department, School of Sciences, Ferdowsi University of Mashhad, Mashhad, 91775-1436, Islamic Republic of Iran.

Received 20 January 2014 – Accepted 3 June 2014

Abstract – The separate contributions of all source regions to organ doses from ^{131}I and ^{123}I administered to the body were calculated using voxelized reference phantoms. The photon and electron components of organ doses were also evaluated for each source region. The MCNPX Monte Carlo particle transport code was utilized for dose calculations. All organs and tissues of male and female phantoms were taken into account as source regions with their corresponding cumulated activities. The results showed that cumulated activities assigned to source regions and inter-organ distances were two factors that strongly affected the contribution of each source to the organ dose. The major contribution of the dose to the main source regions arose from self-irradiation of electrons, while for nearby organs it was due to photons emitted by the main source organs. In addition, self-irradiation plays an important role in the dose delivered to most target organs for lower thyroid uptakes.

Keywords: Internal dose / voxel phantoms / thyroid agents

1 Introduction

Diagnosis of thyroid cancer typically involves a number of procedures and tests. In nuclear medicine, a variety of imaging scans using ^{131}I and ^{123}I are applied to evaluate thyroid nodules for possible thyroid cancer. Estimation of organ doses in these procedures using radioactive iodine is an area of particular concern for radiation protection. This is because the dose coefficient for ^{131}I is quite high. It is not possible to measure organ doses directly, but they can be assessed using Monte Carlo simulations, biokinetic models and computational phantoms.

A comprehensive set of biokinetic data and organ doses for a large number of radiopharmaceuticals was published by ICRP Publication 53 (ICRP, 1988). A number of minor corrections of older data were also provided in the addenda to Publication 53 (ICRP, 1998, 2008) in which the biokinetic data of ^{131}I and ^{123}I remained unaltered.

Stylized phantoms have contributed significantly to radiation dosimetry in nuclear medicine, but their relatively simplistic representation of human anatomy also allows for the possibility of dose estimations that are not completely realistic. With the transition from mathematical to voxel phantoms, the topology of organs and body changed. Two new voxel models, the male and female adult reference computational phantoms, were published by the ICRP Publication 110 (ICRP, 2009) to improve the realism of the human anatomy. This is important especially in internal dosimetry calculations where target organ doses are sensitive to inter-organ distances.

* mirihakim@ferdowsi.um.ac.ir

In the previous paper, absorbed doses from ^{131}I and ^{123}I sodium iodide in voxel phantoms were calculated and compared with the values obtained for the corresponding stylized phantoms (Hoseinian-Azghadi *et al.*, 2013). In this study, further details about the contributions of photons and electrons to organ doses from each source region are assessed and discussed for ^{131}I and ^{123}I.

2 Materials and methods

2.1 Estimation of organ doses

The assessment of the absorbed dose from internal emitters is based on the MIRD (Medical Internal Radiation Dose) formalism (Bolch *et al.*, 2009) and the use of reference phantoms. The following are the equations established from the MIRD formalism for the calculation of the absorbed dose to a target organ, $D(r_T)$:

$$D(r_T) = \sum_{r_S} S(r_T \leftarrow r_S)\tilde{A}(r_S) \quad (1)$$

where the summation over r_S is intended to account for contributions from all source organs to the target organ, $S(r_T \leftarrow r_S)$ (Gy.Bq^{-1}s^{-1}) is the S factor and $A(r_S)$ is the cumulated activity in a source region (Bq.s). The S factor takes into account the radiation type, the energy emitted per transformation, the mass of the target organ and the geometry of the phantom. The cumulated activity is the integral of the time-dependent activity in the source region depending on the administered activity,

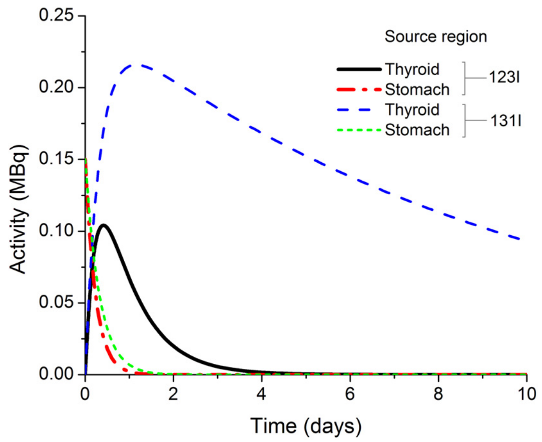

Fig. 1. Time-dependent activity in the source organs (thyroid and stomach) with the assumption of 25% thyroid uptake.

the physical half-life and the biokinetics of the radiopharmaceutical. Mathematically, this type of activity/time curve can be represented by the equation:

$$\tilde{A}(r_S) = \int A(r_S, t)dt \tag{2}$$

where $A(r_S, t)$ is the activity in the source organ, S at time t. This data was obtained from a compartmental biokinetic model in the organs of interest (see Fig. 1). On the basis of this approach, the absorbed dose delivered to the target organ could be obtained for the total disintegrations occurring in the source region.

2.2 ICRP reference phantoms

In this work, the organ doses were calculated in adult male and female ICRP reference voxel phantoms. The organ masses and body dimensions of each phantom matched the reference values reported by ICRP Publication 89 (ICRP, 2002). The densities and elemental compositions for organs and tissues provided in the ICRP Publication 110 (ICRP, 2009) were used in the Monte Carlo simulations.

2.3 Monte Carlo calculations

In order to estimate the S values, Monte Carlo calculations were performed. The source organs were defined in the input file in accordance with standard biokinetic data reported in ICRP Publication 53 (ICRP, 1988). Figure 2 shows cumulated activities for all organs and tissues of the male phantom for 15% thyroid uptake in a coronal section (at y = 12 cm). The spectra published in ENSDF decay data with yields >0.1% were employed. The outputs of MCNPX simulations were the heating tally (tally F6 in the MCNPX code) for photons (kerma approximation) and energy deposition (tally + F6) for electrons. All simulations were performed for 10^7 histories. Thus, a maximum statistical uncertainty of 2% was assured for large organs, while it was up to 6% for small organs, with a volume smaller than 20 cm^3. Finally, the MCNPX outputs in megaelectron volts were converted into the absorbed dose in mGy MBq^{-1}.

2.4 Calculation of CLDs

To explain the differences in organ doses with respect to the distance between the source and target organs, we used chord length distributions (CLDs). A CLD is a relative number histogram of distances between the points in the source and target regions.

A two step algorithm was used to produce CLDs. First, indices were randomly sampled from the voxel array, and if they were inside the organ concerned then one point was randomly picked in the selected voxel. The CLDs were generated by randomly sampling 1 million points in each source and target organ and by assessing the distances between pairs.

3 Results

Total absorbed doses to all target organs considered in ICRP Publication 110 (ICRP, 2009) were calculated for incorporated ^{131}I and ^{123}I (sodium iodide). The process of dose calculation was validated by comparing the organ doses calculated in this study with related studies in the literature. The absorbed doses for ^{123}I (25% thyroid uptake) and ^{131}I (55% thyroid uptake) are compared in Tables 1 and 2, respectively. The organ doses calculated in this study were in good agreement with the values reported by Smith *et al.* (2000), Zankl *et al.* (2010, 2011), and Hadid *et al.* (2013) within 7% on average. Some values for wall organs, however, showed larger differences; for example, the urinary bladder wall doses for 25% uptake of ^{123}I were 7.06×10^{-2} (obtained from Zankl *et al.*, 2011) and 3.69×10^{-2} (calculated in this study) mGy (MBq)$^{-1}$ (62% difference).

The calculations in this study were performed assuming the range 0–55% thyroid uptakes, while uptake of 15% was considered as the typical normal uptake of the thyroid. Separate contributions for all source regions from so-called penetrating (photon) and non-penetrating (electron) radiation for a given radionuclide were obtained.

Table 3 shows the total absorbed dose, photon component, thyroid contribution as a source region and self-dose for a few important target organs. It is indicated that the major contribution of the dose to the main source regions is due to the self-irradiation of electrons. For example, the self-dose of the stomach wall is about 94% and 92% from ^{131}I and ^{123}I, respectively. It should be noted that according to ICRP Publication 100 (ICRP, 2006) only a small cell layer of the stomach wall is considered as the target region rather than the whole wall defined in voxel models. However, Phipps *et al.*'s (2007) results showed that the stomach and colon doses tend to be lower under the ICRP 100 human alimentary tract model.

One expected that the major contribution of the dose to the nearby organs such as the lungs would arise from photons emitted by the thyroid. Figure 3 shows the lung dose and the contribution of the thyroid to that for 0–55% uptakes. It is indicated that for more than 5% uptakes the major contribution of the dose delivered to the lungs is due to the thyroid.

Unexpectedly, this trend is similar for the liver, which is not adjacent to the thyroid (Fig. 4). The percentage contributions to the liver dose from source regions are plotted in this figure. One could expect that photons emitted by the stomach

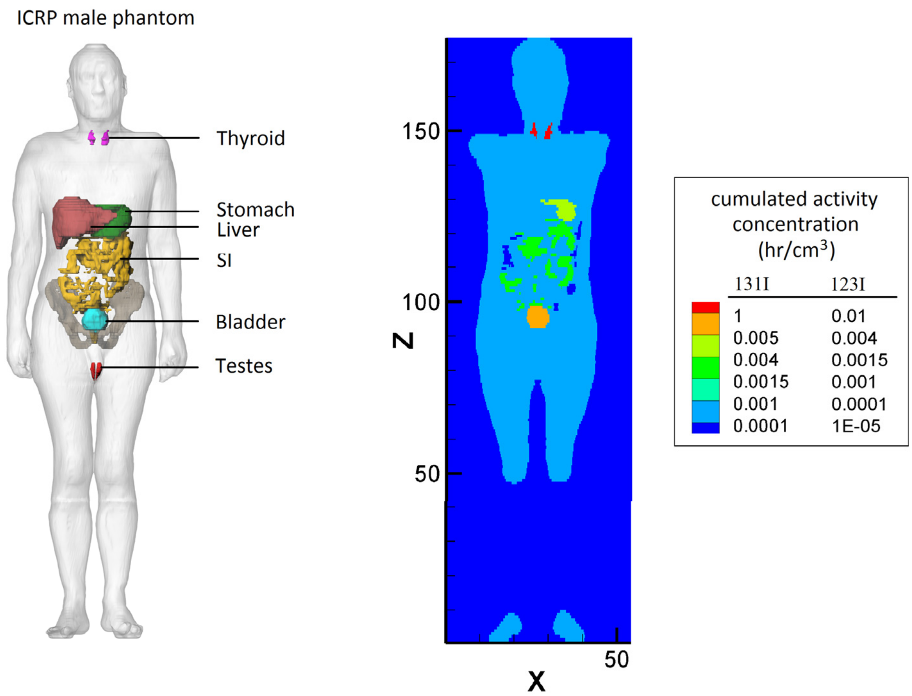

Fig. 2. (Left) adult male ICRP reference phantom and (right) the cumulated activity concentrations of ^{131}I and ^{123}I in a coronal view (at y = 12 cm) of the phantom; a thyroid uptake of 15% is assumed.

are the major contributors. However, this figure shows that for more than 15% uptakes, the contribution of the thyroid to the liver dose is dominant. In the case of lower uptakes, the contribution of the self-dose is greater. Normal values of fractional thyroid uptake varied between 5%–25% and were considered to encompass a range appropriate to the adult euthyroid population of the United States (ICRP, 1988). The absorbed dose to the liver for 15% thyroid uptake as the typical normal uptake is analyzed further in Figure 5. The column chart in this figure shows the contributions of source regions to the total dose of the liver as a typical target organ. Only 35% but still the major contribution of the liver dose is due to the thyroid. 30% of the liver dose is related to its total self-dose, and the contribution of electrons is almost 22%. Photons emitted by the stomach, small intestine (SI), adipose tissue and muscles contribute about 14%, 6%, 4% and 3% to the liver dose, respectively, while it is less than 2% for other source regions.

This issue is observed for organs which are close to the other main source regions according to their cumulated activities. For example the irradiation from bladder contents plays an important role in the dose delivered to the bladder wall, prostate, ovaries and uterus. The contributions of electrons emitted in bladder contents to the bladder wall dose are about 60% and 83% for ^{131}I and ^{123}I, respectively. The percentage contributions from the source regions to the prostate dose are compared in Figure 6. The urinary bladder content for the full range of uptakes is the major source region which exposes the prostate to radiation emitted by ^{131}I.

The major contribution of the dose absorbed in some organs such as the testes is the self-dose (Fig. 7). The electron component of the testes dose is 50% of the total organ dose for ^{131}I. Only 10% of the testes dose is due to bladder contents and less than 0.5% is caused by the thyroid gland. In the case of ^{123}I administration, self-irradiation is still predominant (33% of the total dose). In addition, the contribution of bladder contents, muscles and adipose tissue to the testes dose is noticeable.

The effectiveness of correcting the dose for a real person evaluated with the reference phantom could be estimated by applying a target massbased coefficient for the thyroid. For this purpose, a linear fit was performed on the dose data of AM and AF ICRP phantoms together with a MIRD phantom. The following equation was obtained for 15% uptake:

$$\text{DThyroid}\,(\text{mGy/MBq}) = -11.21\,\text{MThyroid}\,(\text{grams}) + 433.2$$

where DThyroid (mGy/MBq) is the thyroid dose and MThyroid (grams) is the mass of the thyroid gland. This coefficient corrects the thyroid dose according to the real mass of the gland.

4 Discussion

According to the results, the comparison of wall organs showed large differences. The possible factors influencing the observed differences in the organ doses are as follows.
(1) Differences in the method of dose calculation. MIRD formalism was implied in this study in which the S values are derived from Monte Carlo calculation, while in the other studies the SAF method and ICRP Publication 30 (ICRP, 1982) approach were used. The first method is based on photon and electron SAFs and in the latter it is assumed that the energy of electrons is absorbed locally. The electron transport is particularly important for wall organs, which are main source regions, such as the stomach wall or are adjacent to main source regions, such as the urinary bladder wall.

Table 1. Organ doses (mGy/MBq) for 25% thyroid uptake of ^{123}I sodium iodide compared with related studies in the literature.

Authors	Smith *et al.* (2000)		Zankl *et al.* (2010)							Zankl *et al.* (2011)		This study		ICRP 53
Monte Carlo Code										EGSnrc		MCNPX 2.4		
Decay data	ICRP 38		ICRP 107							ICRP 107		ENSDF decay data		ICRP 38
Method of calculation	SAF		SAF							ICRP 30	SAF	MIRD Formalism		MIRD Formalism
Phantom	Golem	MIRD Normalized	Frank	Golem	Visible human	Voxel man	Donna	Helga	Irene	AM ICRP		AM ICRP	AF ICRP	MIRD
Colon	1.31E-02	1.42E-02	1.26E-02	1.31E-02	1.36E-02	2.00E-02	1.30E-02	1.24E-02	1.34E-02	1.22E-02	1.23E-02	1.20E-02	1.22E-02	1.50E-02
Lung	1.22E-02	6.39E-03	1.15E-02	1.21E-02	1.17E-02	1.41E-02	1.09E-02	1.27E-02	1.39E-02	1.15E-02	1.14E-02	1.31E-02	1.47E-02	6.10E-03
Stomach wall	1.18E-01	2.00E-01	1.65E-01	1.75E-01	1.77E-01	2.09E-01	1.76E-01	1.97E-01	1.79E-01	1.63E-01	1.62E-01	7.71E-02	8.46E-02	6.80E-02
Breast	—	—	—	—	—	—	5.35E-03	4.24E-03	6.90E-03	4.81E-01	4.80E-01	4.79E-03	6.32E-03	5.00E-03
Testes	4.93E-03	5.70E-03	—	4.90E-03	4.74E-03	8.20E-03	—	—	—	4.79E-03	4.79E-03	4.66E-03	—	5.20E-03
U bladder wall	5.59E-02	7.06E-02	5.38E-02	4.83E-02	7.73E-02	4.62E-02	7.67E-02	8.73E-02	9.83E-02	7.06E-02	3.74E-02	3.69E-02	3.86E-02	6.90E-02
Liver	9.73E-03	6.33E-03	1.07E-02	9.73E-03	8.42E-03	1.04E-02	9.00E-03	1.01E-02	9.51E-03	9.05E-03	9.05E-03	8.97E-03	1.07E-02	6.30E-03
Thyroid	2.44	3.47	3.08	3.08	3.09	3.1	3.65	3.59	3.59	3.15	3.11	2.94	3.46	3.20E+00

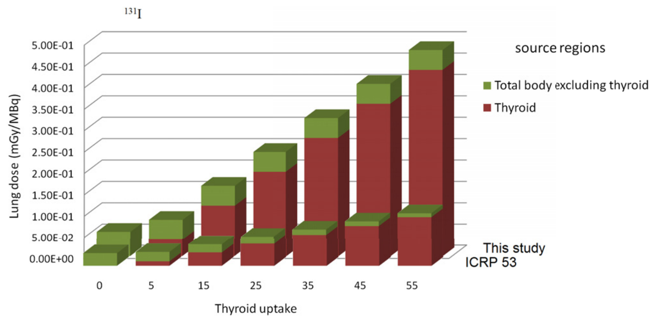

Fig. 3. Absorbed dose to the lungs due to the thyroid (red) and the total body excluding the thyroid (green) versus thyroid uptakes from this study and ICRP Publication 53.

(2) The use of different Monte Carlo codes and photon cross-sections.

In addition, the comparison showed that the relative contributions of source organs and particles change due to exchanging the former stylized phantoms with voxel phantoms. Considering that both the stylized and ICRP voxel phantoms have organ masses matched to the reference man, the differences in these values are likely a consequence of differences in organ placements and organ shapes between the phantoms. Figure 3 shows that the lung dose for thyroid uptake of ^{131}I in ICRP Publication 53 (ICRP, 1988) is smaller than those in this study for voxel phantoms. The thyroid is the major contributor to the lung dose; hence the shorter distances between the thyroid and lungs for voxel phantoms would result in a greater lung dose. Lamart *et al.* (2011) reported the CLDs between the lungs and thyroid in female phantoms which have different mean distances; (14.5 and 20.4 cm) for the ICRP voxel and ORNL phantom, respectively. This shift demonstrates the approximately fourfold greater *lung dose* for the voxel phantoms.

The results showed that the major contribution of the dose to the nearby organs arises from photons emitted by the main source regions. By increasing the thyroid gland uptake, the cumulated activity increases and so the main source organ is the thyroid which exposes other organs to radiation emitted from radioactive iodine. It seems that the effect of self-irradiation on organ doses could be considerable when thyroid uptake is less than 15%. The cumulated activity of the urinary bladder contents decreases with increasing thyroid uptake. Therefore, the contribution from the urinary bladder contents to organ doses has a decreasing trend. This is indicated for the prostate dose in Figure 6.

In general, the contribution of each source to the organ dose is mainly governed by the cumulated activity assigned to the source organ and the distance between two organs. The latter was shown as CLDs for the selected source region and target organ pairs. Increasing the distance between the source and target organ decreases the contribution of the source region to the dose. This issue is indicated for the testes as a target organ in Figures 7 and 8. Despite the greater distance between the liver as a target region and the thyroid as a source region compared with the liver-stomach and liver-small intestine distances the contribution of the thyroid to the liver dose is more than the doses due to the stomach and small intestine. This could be explained by the cumulated activity assigned to the thyroid,

Table 2. Organ doses (mGy/MBq) for 55% thyroid uptake of ^{131}I sodium iodide compared with related studies in the literature.

Authors	**Hadid *et al.* (2013)**				**This study**		**ICRP 53**
Monte Carlo Code	MCNPX 2.6				MCNPX 2.4		
Decay data	ICRP 38		ICRP 107		ENSDF decay data		ICRP 38
Method of calculation	MIRD Formalism		MIRD Formalism		MIRD Formalism		MIRD Formalism
Phantom	AM ICRP	AF ICRP	AM ICRP	AF ICRP	AM ICRP	AF ICRP	MIRD
Colon	5.88E-02	4.91E-02	5.69E-02	4.79E-02	5.59E-02	4.86E-02	4.80E-02
Lung	4.83E-01	5.29E-01	4.66E-01	5.12E-01	4.83E-01	5.31E-01	1.30E-01
Stomach wall	1.71E-01	1.67E-01	1.65E-01	1.63E-01	5.95E-01	6.29E-01	4.60E-01
Breast	8.96E-02	2.36E-01	8.76E-02	2.27E-01	9.30E-02	2.27E-01	9.10E-02
Testes	2.19E-02	4.84E-02	2.26E-02	4.65E-02	2.23E-02	5.33E-02	2.60E-02
U bladder wall	8.44E-02	9.98E-02	8.35E-02	9.67E-02	8.88E-02	1.00E-01	2.90E-01
Liver	1.07E-01	1.15E-01	1.03E-01	1.11E-01	1.03E-01	1.11E-01	4.30E-02
Thyroid	7.53E+02	8.87E+02	7.55E+02	8.89E+02	7.56E+02	8.90E+02	7.90E+02

Table 3. Organ doses (mGy/MBq) for 15% thyroid uptake of ^{131}I and ^{123}I sodium iodide in male and female phantoms. The photon component in the organ dose, the contribution of some important source organs to the organ dose and the selfdose were tabulated.

	Target organs	**^{131}I Dose (mGy/MBq)**	**Photon**	**Thyroid**	**Source organ contributing most**	**^{123}I Dose (mGy/MBq)**	**Photon**	**Thyroid**	**Source organ contributing most**
Male phantom	Colon	4.85E-02	73%	8%	25% self-dose	1.22E-02	91%	1%	32% SI
	Lung	1.67E-01	82%	71%	18% self-dose	1.14E-02	76%	25%	40% self-dose
	Stomach wall	5.56E-01	19%	3%	94% Stomach	7.76E-02	46%	0%	92% Stomach
	Breast	4.41E-02	70%	42%	30% self-dose	4.62E-03	75%	7%	31% self-dose
	Testes	2.33E-02	50%	0%	55% self-dose	4.67E-03	77%	0%	33% self-dose
	Urinary bladder wall	1.40E-01	70%	0%	82% Bladder Cont.	4.06E-02	95%	0%	85% Bladder Cont.
	Liver	5.33E-02	77%	35%	30% self-dose	8.72E-03	88%	4%	31% self-dose
	Thyroid	2.07E+02	6%	100%	100% self-dose	1.78E+00	24%	99%	99% self-dose
Female phantom	Colon	4.92E-02	70%	3%	30% self-dose	1.25E-02	90%	0%	37% SI
	Lung	1.84E-01	80%	71%	22% self-dose	1.27E-02	74%	25%	42% self-dose
	Stomach wall	5.92E-01	18%	2%	95% Stomach	8.36E-02	47%	0%	92% Stomach
	Breast	8.15E-02	81%	67%	22% self-dose	5.59E-03	76%	18%	40% self-dose
	Ovaries	6.01E-02	75%	1%	36% self-dose	1.70E-02	93%	0%	44% Bladder Cont.
	Urinary bladder wall	1.57E-01	65%	0%	78% Bladder Cont.	4.20E-02	95%	0%	81% Bladder Cont.
	Liver	5.98E-02	75%	32%	31% self-dose	1.04E-02	88%	3%	34% self-dose
	Thyroid	2.43E+02	6%	100%	100% self-dose	2.08E+00	24%	100%	100% self-dose

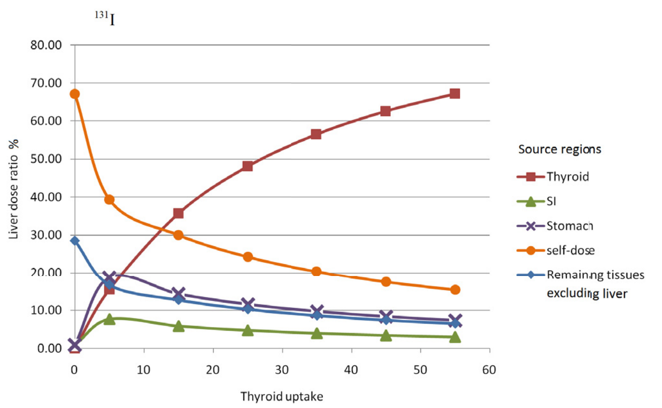

Fig. 4. The contributions of each source region to the liver dose with respect to thyroid uptake for ^{131}I incorporated in a male phantom.

which is higher than other regions. Figure 2 shows the cumulated activity concentrations in a coronal section of a male phantom in units of h/cm^3. The main source regions and remaining tissues are specified in this figure.

To go further in the interpretation of the results, the influence of the type and the energy of emitted particles was studied. The electron component of self-doses for ^{131}I is greater than that for ^{123}I. This is due to the fact that ^{123}I decay by electron capture and the subsequent Auger and conversion electrons have lower energies (energy of 3.19 keV with yields of 0.95), while electrons emitted by ^{131}I are a consequence of its beta decay (mean energy of 192 keV with yields of 0.90).

Additionally, the physical half-life of ^{131}I is 8.02 days while it is 13.27 hours for ^{123}I and so the effective half-life of the former radionuclide is longer. This yields a greater value of time-integrated activity for ^{131}I (*i.e.* longer residence time of ^{131}I). Because of the greater cumulated activity of the thyroid as the most important source organ, the contribution of organ doses caused by the thyroid source is higher for ^{131}I than that for ^{123}I. As a consequence of its short half-life, the activity concentrated in the thyroid is less significant for ^{123}I. Thus, the

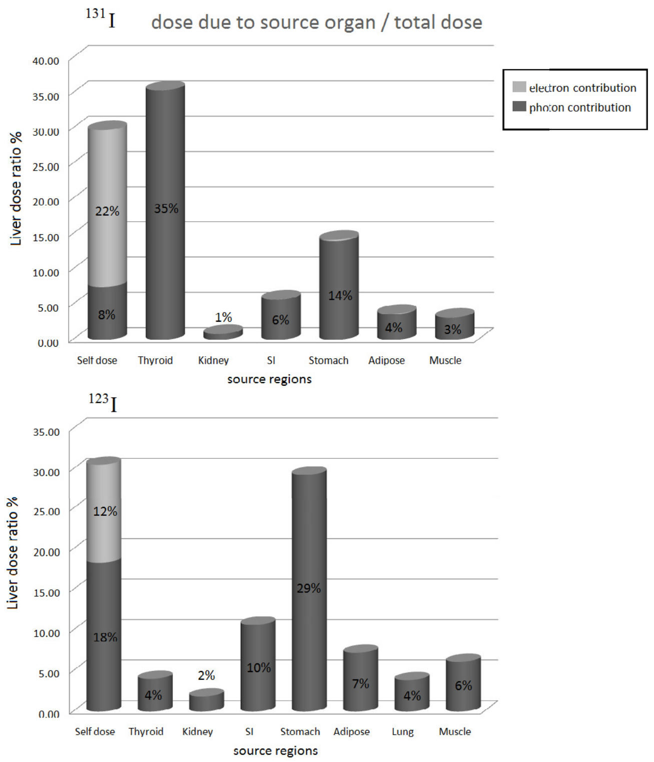

Fig. 5. Electron (light gray) and photon (dark gray) contributions of each source region to the liver dose for ^{131}I and ^{123}I incorporated in a male phantom assuming 15% thyroid uptake.

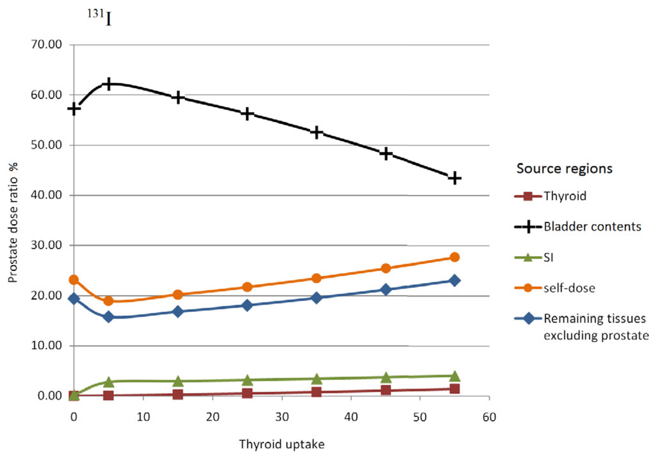

Fig. 6. The contributions of each source region to the prostate dose with respect to thyroid uptake for ^{131}I incorporated in a male phantom.

contribution of the stomach to the liver dose is greater for ^{123}I (29%) while this value is 14% for administration of ^{131}I.

Except for the self-dose, the electron component of the organ dose is negligible. This is due to local absorption of electrons in the source organ. For source-target pairs such as the skin-testes which are located very close to each other, the electron contribution to the testes dose is about 0.7%.

The contribution of the urinary bladder contents is more than that of muscles and adipose tissue to the testes dose for

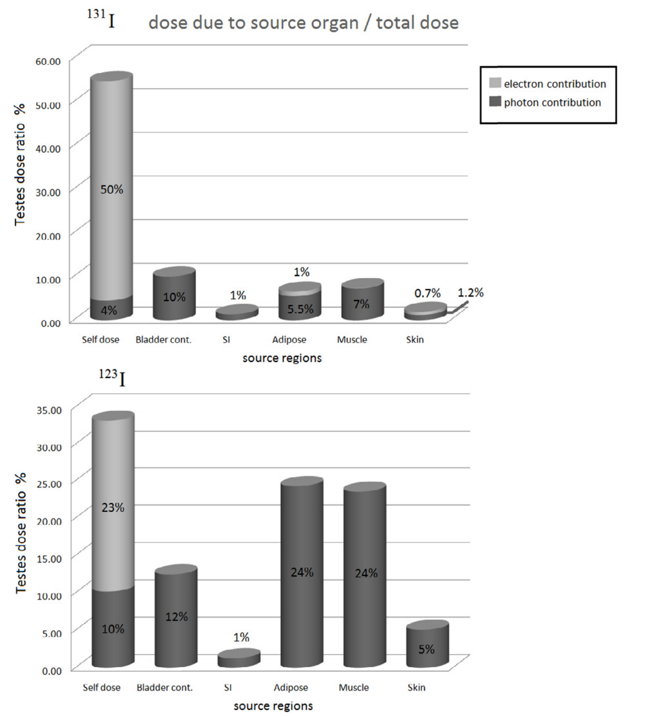

Fig. 7. Electron (light gray) and photon (dark gray) contributions of each source region to the testes dose for ^{131}I and ^{123}I incorporated in a male phantom assuming 15% thyroid uptake.

^{131}I. This trend is reversed for ^{123}I. These are the results of: (i) the greater cumulated activity assigned to the urinary bladder for ^{131}I than that for ^{123}I (1.6-fold); and (ii) the higher energy of photons emitted by ^{131}I (energy of 364 keV with yields of 0.82) than that by ^{123}I (energy of 159 keV with yields of 0.83).

According to our analyses the differences in self-doses are primarily due to differences in the organ masses. Only the thyroid dose is completely a self-dose. So, the thyroid dose could be evaluated for a real person using the reference phantom data by applying a target massbased coefficient. The differences among other organ doses are mainly governed by inter-organ distances between the source and target pairs and the auto-absorbed dose correction could not be applied for them.

Since the lifetime probability coefficient for fatal cancer for workers is 4×10^{-2}/Sv (ICRP, 1991; Wang *et al.*, 2014), it may imply that a typical thyroid scan with 8-mCi administered activity may induce a secondary cancer risk in the thyroid and its adjacent organs as listed in Table 4 for administration of ^{131}I. The secondary risk factors for ^{123}I were less than 0.5%, so they were eliminated from this table.

5 Conclusion

Our analysis showed that the contribution of each source to the organ dose was strongly correlated with the cumulated activities (assigned to source regions) as well as inter-organ distances as demonstrated by differences in the mean, standard deviation and shape of the CLDs. The latter is important especially in internal dosimetry calculations where target organ

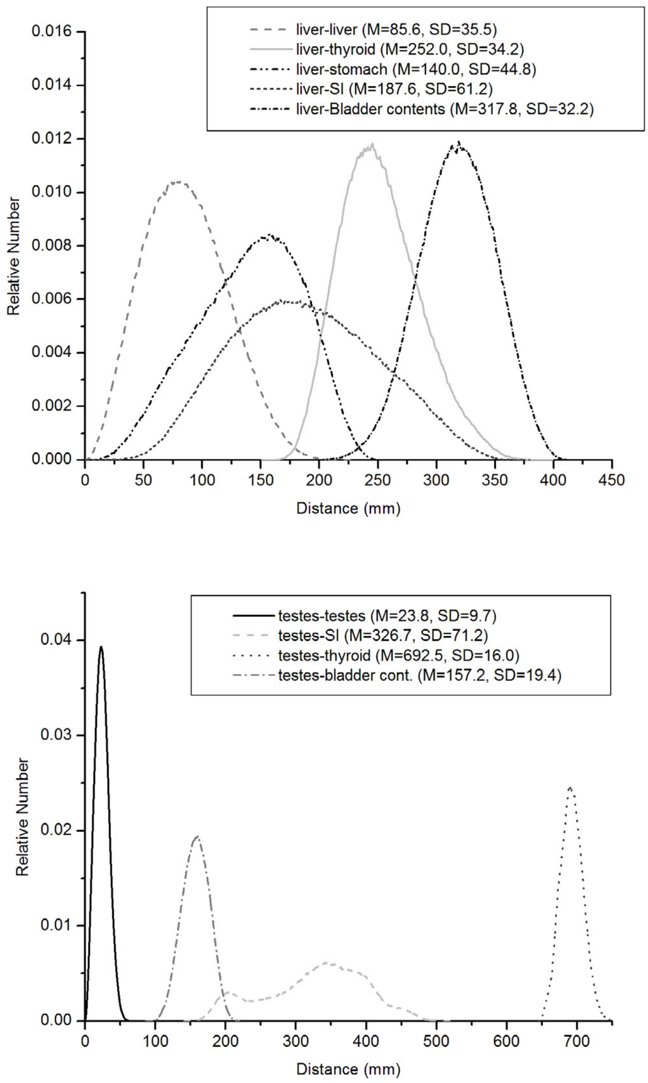

Fig. 8. Comparison of CLDs for target-source pairs in a male phantom. M and SD in the legend stand for mean and standard deviation, respectively.

Table 4. Risk assessment for secondary cancer in the thyroid after 8 mCi administered activity of ^{131}I for a thyroid scan. The absorbed dose, tissue weighted dose to the thyroid (effective dose) and the corresponding risk factor were tabulated for a range of 0% to 55% thyroid uptake.

	Thyroid uptake	Absorbed dose (mGy/MBq)	Effective dose (Sv/MBq)	Secondary cancer risk (%) due to 8 mCi
^{131}I-Thyroid	0%	1.20E-02	4.82E-07	0
	5%	6.85E+01	2.74E-03	3
	15%	2.06E+02	8.26E-03	10
	25%	3.44E+02	1.37E-02	16
	35%	4.81E+02	1.92E-02	23
	45%	6.19E+02	2.48E-02	29
	55%	7.56E+02	3.03E-02	36

doses are sensitive to inter-organ distances. The major contribution of the dose to the main source regions is due to self-irradiation of electrons, while for the nearby organs it is due to photons emitted by the main source organs. The major contribution of the dose absorbed in some organs that are not close enough to the main source regions is the self-dose. The comparisons showed, in general, some differences between ^{131}I and ^{123}I in the contribution of each source to the organ dose. The type and the energy of emitted particles are other factors influencing the observed differences.

The outcome of this study regarding risk assessment and radiation protection for patients of nuclear medicine is the secondary cancer risk probabilities with respect to the thyroid uptake. It should be useful for medical doctors performing or requesting thyroid scans involving radioiodine.

Acknowledgements. This work was supported by the Vice President for Research & Technology of Ferdowsi University of Mashhad (Grant No. 20425, 1/3/2012).

References

Bolch W.E., Eckerman K.F., Sgouros G., Thomas S.R. (2009) MIRD pamphlet no. 21: a generalized schema for radiopharmaceutical dosimetry – standardization of nomenclature, *J. Nucl. Med.* **50**, 477-484.

ENSDF Decay Data in the MIRD (Medical Internal Radiation Dose) Format. National Nuclear Data Center: Brookhaven National Laboratory, Upton, N.Y., USA. http://www.orau.org/ptp/PTP%20Library/library/DOE/bnl/nuclidedata/MIRI131.htm (1 January 2014, date last accessed).

Hadid L., Gardumi A., Desbrée A. (2013) Evaluation of absorbed and effective doses to patients from radiopharmaceuticals using the ICRP 110 reference computational phantoms and ICRP 103 formulation, *Radiat. Prot. Dosim.* **156** (2), 141-159.

Hoseinian-Azghadi E., Rafat-Motavalli L., Miri-Hakimabad H. (2013) Internal dosimetry estimates using voxelized reference phantoms for thyroid agents, *J. Radiat. Res.* **55** (3), 407-422.

ICRP Publication 30 (1982) Limits for Intakes of Radionuclides by Workers, *Ann. ICRP* **8** (4).

ICRP Publication 38 (1983) Radionuclide Transformations – Energy and Intensity of Emissions, *Ann. ICRP* **11-13**.

ICRP Publication 53 (1988) Radiation dose to patients from radiopharmaceuticals, *Ann. ICRP* **18** (1-4).

ICRP Publication 60 (1991) Recommendations of the International Commission on Radiological Protection, *Ann. ICRP* **21** (1-3).

ICRP Publication 80 (1998) Radiation Dose to Patients from Radiopharmaceuticals (Addendum to ICRP Publication 53), *Ann. ICRP* **28** (3).

ICRP Publication 89 (2002) Basic anatomical and physiological data for use in radiological protection: reference values, *Ann. ICRP* **32** (3-4).

ICRP Publication 100 (2006) Human alimentary tract model for radiological Protection, *Ann. ICRP* **36** (1-2).

ICRP Publication 106 (2008) Radiation Dose to Patients from Radiopharmaceuticals – Addendum 3 to ICRP Publication 53, *Ann. ICRP* **38** (1-2).

ICRP Publication 107 (2008) Nuclear Decay Data for Dosimetric Calculations, *Ann. ICRP* **38** (3).

ICRP Publication 110 (2009) Adult Reference Computational Phantoms, *Ann. ICRP* **39** (2).

Lamart S., Bouville A., Simon S.L., Eckerman K.F., Melo D., Lee C. (2011) Comparison of internal dosimetry factors for three classes of adult computational phantoms with emphasis on I-131 in the thyroid, *Phys. Med. Biol.* **56** (22), 7317-7335.

Phipps A.W., Fell T.P., Harrison J.D., Paquet F., Leggett R.W. (2007) Dose coefficients calculated using the new ICRP model for the human alimentary tract, *Radiat. Prot. Dosim.* **127** (1-4), 79-85.

Smith T., Petoussi-Henss N., Zankl M. (2000) Comparison of internal radiation doses estimated by MIRD and voxel techniques for a 'family' of phantoms, *Eur. J. Nucl. Med.* **27** (9), 1387-1398.

Wang J.N., Lee K.W., Jiang S.H. (2014) Effective dose evaluation for BNCT brain tumor treatment based on voxel phantoms, *Appl. Radiat. Isotopes* **88**, 55-58.

Zankl M., Petoussi-Henss N., Janzen T., Uusijärvi H., Schlattl H., Li W.B., Giussani A., Hoeschen C. (2010) New calculations for internal dosimetry of beta-emitting radiopharmaceuticals, *Radiat. Prot. Dosim*. **139** (1-3), 245-249.

Zankl M., Schlattl H., Petoussi-Henss N., Hoeschen C. (2011) Voxel phantoms for internal dosimetry. In: *Radiation Physics for Nuclear Medicine* (M.C. Cantone, C. Hoeschen, Eds.), pp. 257-279. Springer, Berlin.

Cite this article as: E. Hoseinian-Azghadi, L. Rafat-Motavalli, H. Miri-Hakimabad. The contributions of source regions to organ doses from incorporated radioactive iodine. Radioprotection 49(4), 249-256 (2014).